

Partial wave analysis of K^+N scattering and the possibility of pentaquark $\Theta^+(1540)$

Kook-Jin Kong · Byung-Geel Yu

January 8, 2022

Abstract Elastic $K^+n \rightarrow K^+n$ and charge exchange $K^+n \rightarrow K^0p$ reactions at low momenta are investigated using the partial wave analysis. Isospin relation gives constraints for the partial s - and p -waves among elastic K^+p , K^+n and charge exchange $K^+n \rightarrow K^0p$ amplitudes. Two sets of the phase shift for these partial waves in the isoscalar channel are obtained from the fit of experimental data on total and differential cross sections. Polarization observable leads to a good criterion to decide which set is valid. Differential cross section data near $P_{\text{Lab}} = 434$ MeV/ c suggests a possibility of a resonance, e.g., the exotic $\Theta^+(1540)$ baryon around $\sqrt{s} \simeq 1.54$ GeV.

PACS 11.80.Et, 13.75.Jz, 13.85.Dz, 14.20.Pt

1 Introduction

According to the conventional quark model, a meson consists of $\{q\bar{q}\}$ and a baryon of $\{qqq\}$ or $\{\bar{q}\bar{q}\bar{q}\}$. However, other states called the tetraquark $\{q\bar{q}q\bar{q}\}$ and pentaquark $\{qqqq\bar{q}\}$ may also exist [1]. In search of the pentaquark state, the so called $\Theta^+(1540)$ of the $\{uudd\bar{s}\}$ configuration, T. Nakano *et al.* claimed to observe the exotic baryon resonance in the reaction $\gamma n \rightarrow K^+K^-n$ on the ^{12}C target at 1.54 ± 0.01 GeV with the width less than 25 MeV [2], though more rigorous verification awaits since then. A recent experiment using photon beam reported a narrow peak at the missing mass around 1.54 GeV which could be the $\Theta^+(1540)$ state in

the reaction $\gamma p \rightarrow pK_S K_L$ [3]. As the pentaquark configuration needs the $K^+\{u\bar{s}\}$ and neutron $\{udd\}$, the elastic $K^+n \rightarrow K^+n$ and charge exchange $K^+n \rightarrow K^0p$ reactions have long been the candidates of finding the $\Theta^+(1540)$ predicted at mass $M \approx 1.53$ GeV/ c^2 with the width $\Gamma < 15$ MeV [4, 5]. The correction for the width was later suggested in Refs. [6, 7]. More recently, a theoretical study of the reaction $K^+d \rightarrow K^0p(p)$ predicted the $\Theta^+(1540)$ peak most probable at $P_{\text{Lab}} \approx 0.4$ GeV/ c [8]. In this regard, the K^+N reaction [9, 10, 11] is intuitive to investigate the possibility of finding the exotic baryon, $\Theta^+(1540)$.

Beyond the resonance region up to tens of GeV in the K^+N reaction, the peripheral scattering via the t -channel meson exchange becomes dominant, and the reaction mechanism is found to be governed by the tensor meson f_2 and Pomeron exchanges in the isoscalar channel [12]. In the low momentum region below the kaon laboratory momentum $P_{\text{Lab}} \leq 800$ MeV/ c , the meson exchange alone is not appropriate to describe the differential and total cross-sections. Therefore, we try to understand the K^+N reaction by using the partial wave analysis from threshold up to $P_{\text{Lab}} \approx 800$ MeV/ c with our particular interest in the region around $P_{\text{Lab}} = 434$ MeV/ c where the pentaquark $\Theta^+(1540)$ is expected to exist.

In previous works there is a significant disagreement between theory and experiment in the reaction cross sections near $P_{\text{Lab}} \approx 434$ MeV/ c . A. Sibirtsev *et al.* [13] calculated the K^+d cross section using the single scattering impulse approximation to find a large discrepancy with data around $P_{\text{Lab}} = 434$ MeV/ c in the case of the K^+n elastic reaction. Furthermore, K. Aoki *et al.* [14] investigated the K^+N cross section by employing the wave function renormalization method and obtained the result inconsistent with experiment near

Kook-Jin Kong · Byung-Geel Yu
Research Institute of Basic Science, Korea Aerospace University,
Goyang, 10540, Korea
E-mail: bgyu@kau.ac.kr

$P_{\text{Lab}} = 434 \text{ MeV}/c$. All these numerical consequences are interesting in the sense that they require a new approach to the region where the $\Theta^+(1540)$ is predicted to exist.

In this paper we will first work with the isovector amplitude from the low momentum elastic K^+p reaction, in which case only the s -wave is considered from the isotropy of the reaction except for the Coulomb repulsion at very forward angles. After doing this, we will extract the isoscalar amplitudes from the elastic $K^+n \rightarrow K^+n$ and charge exchange $K^+n \rightarrow K^0p$ reactions to investigate whether the isoscalar exotic $\Theta^+(1540)$ exists in the expected region. Though starting from a simple fit of parameters for the s -wave phase shift for the K^+p elastic reaction, the current approach is of value to describe the reaction cross sections for the three channels with the phase shift of partial waves in a unified way.

The paper is organized as follows. In Sec. II, we introduce the reaction mechanism for the K^+N reaction at low momenta in terms of partial waves. Sec. III devotes to a discussion of numerical consequences in total and differential cross sections including polarization observables in comparison with experimental data. In Sec. IV, based on our findings in the present analysis a perspective on the possibility of finding the pentaquark $\Theta^+(1540)$ is given.

2 Partial wave analysis for K^+N reactions

The K^+N reaction consists of following three channels

$$K^+p \rightarrow K^+p, \quad (1)$$

$$K^+n \rightarrow K^0p, \quad (2)$$

$$K^+n \rightarrow K^+n. \quad (3)$$

Since the isospin of kaon is $1/2$ in common with nucleon, the elastic channel $K^+p \rightarrow K^+p$ is composed of the amplitude of isospin $I = 1$, and other two are the mixtures of isospin $I = 1$ and 0 . Therefore, they are expressed as the sum of the isoscalar ($I = 0$) and isovector ($I = 1$) amplitudes which are given by,

$$\mathcal{M}(K^+p \rightarrow K^+p) = \mathcal{M}^{(1)} + \mathcal{M}_C, \quad (4)$$

$$\mathcal{M}(K^+n \rightarrow K^0p) = \frac{1}{2} \left(\mathcal{M}^{(1)} - \mathcal{M}^{(0)} \right), \quad (5)$$

$$\mathcal{M}(K^+n \rightarrow K^+n) = \frac{1}{2} \left(\mathcal{M}^{(1)} + \mathcal{M}^{(0)} \right), \quad (6)$$

where $\mathcal{M}^{(0)}$ ($\mathcal{M}^{(1)}$) is the isoscalar (isovector) component of the reaction amplitude and \mathcal{M}_C is the Coulomb amplitude due to the repulsive interaction between K^+ and proton [14]. Hence, the following relation holds for

these three channels,

$$\begin{aligned} \mathcal{M}(K^+n \rightarrow K^0p) \\ = \mathcal{M}(K^+p \rightarrow K^+p) - \mathcal{M}(K^+n \rightarrow K^+n). \end{aligned} \quad (7)$$

In practice, the experimental data on kaon scattering off a neutron target are obtained from the scattering off a deuteron target $K^+d \rightarrow K^+n(p)$ with the spectator proton [15,16]. Therefore, the formula relevant should be modified to take into account the deuteron form factors I_0 and J_0 [17]. However, as the I_0 's are almost 1 except for the backward region and J_0 's are almost 0 except for the forward region, these form factors can be ignored in the calculation.

Since the elastic channel $K^+p \rightarrow K^+p$ is of pure isovector, we can easily find the isovector amplitude $\mathcal{M}^{(1)}$ in the experimental data below $800 \text{ MeV}/c$. Then, the isoscalar amplitude $\mathcal{M}^{(0)}$ is determined from the isospin relation for the $K^+n \rightarrow K^0p$ and $K^+n \rightarrow K^+n$ reactions in Eq. (7) above.

2.1 Isovector amplitude

In the elastic $K^+p \rightarrow K^+p$ scattering below $P_{\text{Lab}} \approx 800 \text{ MeV}/c$, the total cross section is almost constant in the region. Apart from the Coulomb repulsion, the flatness of the shape is due to the repulsive hadronic interaction between K^+ and nucleon, which gives a hint at the phase shift. In the differential cross section, the angular dependence is isotropic excluding the sharp peaks at very forward angles due to the Coulomb repulsion. To implement such an isotropy in the differential cross section, a partial s -wave is considered with the phase shift. Denoting it by the symbol S_{11} , the isovector amplitude for the s -wave is written as

$$S_{11} = \frac{1}{2ik} \left(\eta_{0+}^1 e^{2i\delta_{0+}^1} - 1 \right) \quad (8)$$

with the inelasticity $\eta_{0+}^1 = 1$ for simplicity.

The phase shift of S_{11} is obtained as a linear function of the incident kaon momentum k in the center of mass frame, i.e.,

$$\delta_{0+}^1(k) = a_0 + b_0 k \quad (9)$$

with the coefficients $a_0 = 3$ and $b_0 = -107 \text{ GeV}^{-1}$ fixed to the differential cross section data [18,19]. The phase shift is negative (see Fig. 5 below) and consistent with the repulsive hadron interaction between K^+ and proton. Our fit in Eq. (9) is almost the same as that of Goldhaber [18], and hence, the total amplitude is given by

$$\mathcal{M}(K^+p \rightarrow K^+p) = S_{11} + \mathcal{M}_C \quad (10)$$

with the Coulomb interaction term \mathcal{M}_C discussed in detail in Ref. [14].

2.2 Isoscalar amplitude

Now that we are dealing with the low momentum reaction below 800 MeV/c, it is good to consider the s and p -waves for the isoscalar amplitude. Similar to the isovector case, the isoscalar s -wave amplitude is denoted as

$$S_{01} = \frac{1}{2ik} \left(\eta_{0+}^0 e^{2i\delta_{0+}^0} - 1 \right), \quad (11)$$

and the partial p -waves are further constructed as,

$$P_{01} = f_{1-}^0 \cos \theta - i\boldsymbol{\sigma} \cdot \hat{n} f_{1-}^0 \sin \theta, \quad (12)$$

$$P_{03} = 2f_{1+}^0 \cos \theta + i\boldsymbol{\sigma} \cdot \hat{n} f_{1+}^0 \sin \theta, \quad (13)$$

where

$$f_{1\pm}^0 = \frac{1}{2ik} \left(\eta_{1\pm}^0 e^{2i\delta_{1\pm}^0} - 1 \right) \quad (14)$$

with $\eta_{0+}^0 = 1$ and $\eta_{1\pm}^0 = 1$ for simplicity.

Thus, from the isospin relations in Eqs. (4), (5) and (6) above, the scattering amplitudes for $K^+n \rightarrow K^+n$ and $K^+n \rightarrow K^0p$ reactions are written in terms of these s and p waves,

$$\mathcal{M}(K^+n \rightarrow K^+n) = \frac{1}{2} (S_{11} + S_{01} + P_{01} + P_{03}), \quad (15)$$

$$\mathcal{M}(K^+n \rightarrow K^0p) = \frac{1}{2} (S_{11} - S_{01} - P_{01} - P_{03}), \quad (16)$$

which satisfies Eq. (7).

For those elastic and charge exchange K^+n reactions above, there are two sets of data on the differential cross section measured by C. J. S. Damerell *et al.* [15] as presented in Fig. 3 and by G. Giacomelli *et al.* [16] in Fig. 4, respectively. Thus, two approaches are possible, and we focus on Damerell's data first to find the isoscalar amplitudes S_{01} , P_{01} and P_{03} in Eqs. (15) and (16). We call this the set I. The other is to fit to Giacomelli's data, then, which is called the set II.

3 Numerical results

3.1 Isovector amplitude

Given the phase shift δ_{0+}^1 for the isovector amplitude S_{11} in Eq. (9), differential cross sections $d\sigma/d\Omega$ for elastic K^+p reaction in the range $150 \leq P_{\text{Lab}} \leq 750$ MeV/c are shown in Fig. 1. The isotropic pattern is clearly exhibited except for the Coulomb repulsion sharply peaked at very forward angles. Figure 2 presents the total cross section where the solid and dashed curves are with and without Coulomb repulsion. Because it is highly divergent as the angle $\theta \rightarrow 0$, we obtain the total cross section by restricting the range of the angle to $-1 < \cos \theta < 0.85$ in the integration of differential cross section. As the s -wave with the phase shift linear in k

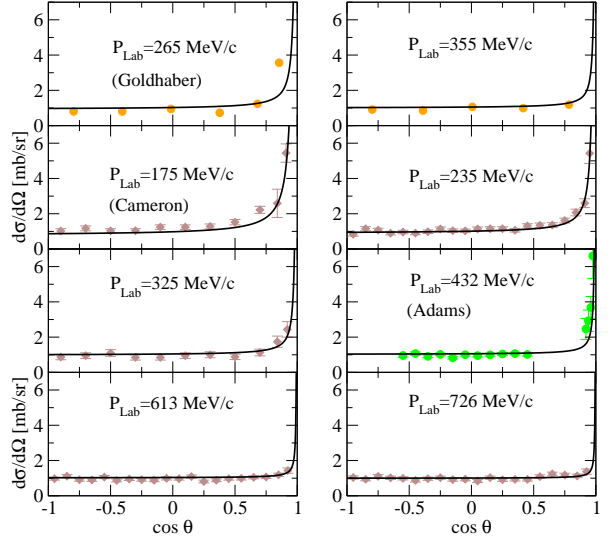


Fig. 1 Differential cross sections for elastic $K^+p \rightarrow K^+p$ reaction at low momenta. The Coulomb repulsion is responsible for the forward peaks in the present calculation. Data in the upper two panels are taken from Refs. [18], [19] and others are from Ref. [20].

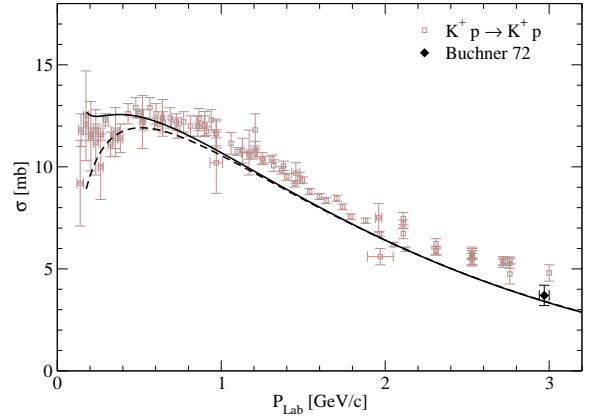


Fig. 2 Total cross section for elastic $K^+p \rightarrow K^+p$ reaction from S_{11} . The solid curve includes the Coulomb effect and the dashed one without it. Data are taken from Particle Data Group.

in Eq. (10) reproduces the total cross section to a degree, the s -wave dominance assumed in the fit is plausible up to 3 GeV/c, even though the anisotropy of the differential cross section becomes stronger above the $P_{\text{Lab}} \geq 800$ MeV/c.

3.2 Isoscalar amplitude

In the case of the isoscalar amplitude, however, since the anisotropy appears in the region $P_{\text{Lab}} \leq 800$ MeV/c as can be seen in Figs. 3 and 4, the p -wave as well as

Table 1 Coefficients a_i, b_i , and c_i for the set I and set II. The subindex $i = 0, 1, 3$ for the isoscalar amplitudes. The values in the left part are for the set I and the other part are for the set II. The coefficient b_i and c_i are in units of GeV^{-1} and GeV^{-3} , respectively.

	a_i	b_i	c_i		a_i	b_i	c_i
δ_{0+}^1	3	-107	-		3	-107	-
δ_{0+}^0	-36	92	100		-36	92	170
δ_{1-}^0	-5	-48	120		-460	1765	-2850
δ_{1+}^0	-12	90	-		-32	94	-

the s -wave should be included in the partial waves S_{01} , P_{01} and P_{03} .

3.2.1 The set I

The parameters for the set I are obtained from the fitting procedure to Damarell's data [15] in Fig. 3. In contrast to the simple form of the S_{11} phase shift in Eq. (9) the parameterization of the phase shift in Eq. (14) for the p -wave is rather complicated due to the inclusion of the k^3 term for the anisotropic angular distribution, i.e.,

$$\begin{aligned}\delta_{0+}^0(k) &= (a_0 + b_0 k_0 + c_0 k_0^3) \times e^{(k-k_0)/m_0}, \\ \delta_{1-}^0(k) &= (a_1 + b_1 k_0 + c_1 k_0^3) \times e^{(k-k_0)/m_0}, \\ \delta_{1+}^0(k) &= (a_3 + b_3 k_0) \times e^{(k-k_0)/m_0}\end{aligned}\quad (17)$$

with $k_0 = 220$ and $m_0 = 100$ MeV/c for $k < 220$ MeV/c , and

$$\begin{aligned}\delta_{0+}^0(k) &= a_0 + b_0 k + c_0 k^3, \\ \delta_{1-}^0(k) &= a_1 + b_1 k + c_1 k^3, \\ \delta_{1+}^0(k) &= a_3 + b_3 k\end{aligned}\quad (18)$$

for $220 \leq k \leq 590$ MeV/c , and

$$\begin{aligned}\delta_{0+}^0(k) &= (a_0 + b_0 k_1 + c_0 k_1^3) \times e^{-(k-k_1)/m_1}, \\ \delta_{1-}^0(k) &= (a_1 + b_1 k_1 + c_1 k_1^3) \times e^{-(k-k_1)/m_1}, \\ \delta_{1+}^0(k) &= (a_3 + b_3 k_1) \times e^{-(k-k_1)/m_1}\end{aligned}\quad (19)$$

for $k > 590$ MeV/c with $k_1 = 590$ and $m_1 = 1500$ MeV/c . We use the function exponentially decreasing outside of the interval. The continuity of the amplitude should provide a boundary condition between two different momentum regions in order to constrain the coefficients a_i, b_i and c_i further. They are listed in the left part of Table 1.

3.2.2 The set II

Giacomelli's data [16] in Fig. 4 are used to fix the parameters of the set II. As before, the phase shifts $\delta_{0+}^0(k)$, $\delta_{1-}^0(k)$ and $\delta_{1+}^0(k)$ are expressed the same as in Eq. (17) for $k < 335$ MeV/c with $k_0 = 335$ and $m_0 = 50$ MeV/c ,

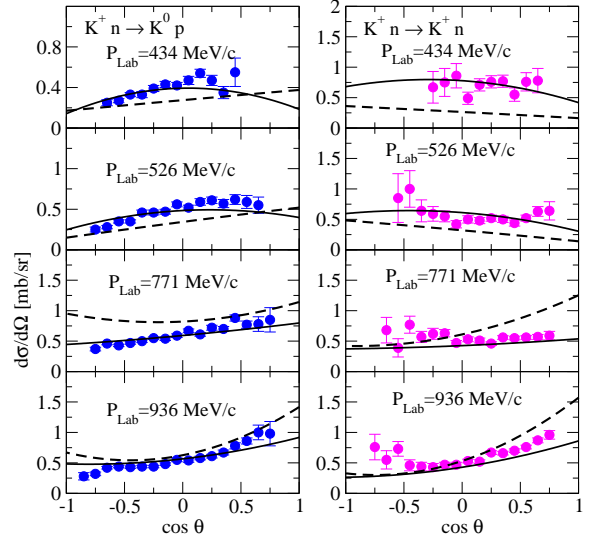


Fig. 3 Differential cross sections for $K^+n \rightarrow K^0p$ (left) and for $K^+n \rightarrow K^+n$ (right). The solid curve results from the set I and the dashed one from the set II, respectively. Data are taken from Ref. [15].

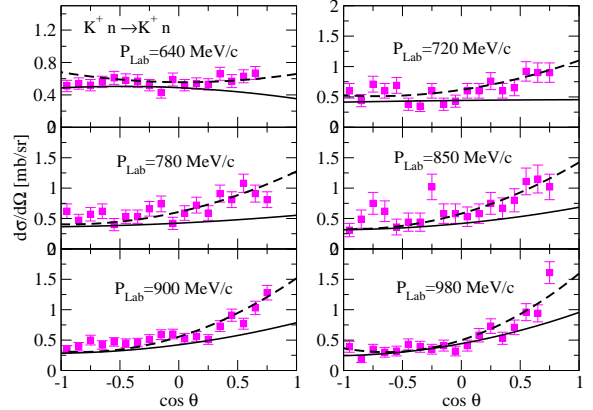


Fig. 4 Differential cross sections for $K^+n \rightarrow K^+n$ elastic scattering. Notations are the same as in Fig. 3. Data are taken from Ref. [16].

and as in Eq. (18) for $335 \leq k \leq 540$ MeV/c , and as in Eq. (19) for $k > 540$ MeV/c with $k_1 = 540$ and $m_1 = 3000$ MeV/c with the parameters a_i, b_i and c_i listed in the right part of Table 1.

Differential cross sections for elastic and charge exchange K^+n interactions are analyzed in Figs. 3 and 4 based on the parameter sets I and II. Given the different set of experimental data by Damerell [15] and Giacomelli [16], the description of the cross section from the set I is better than that from the set II in Fig. 3, whereas this tendency is opposite in Fig. 4. The differential cross sections at $P_{\text{Lab}} = 434$ and 526 MeV/c are of particular importance to look for the $\Theta^+(1540)$

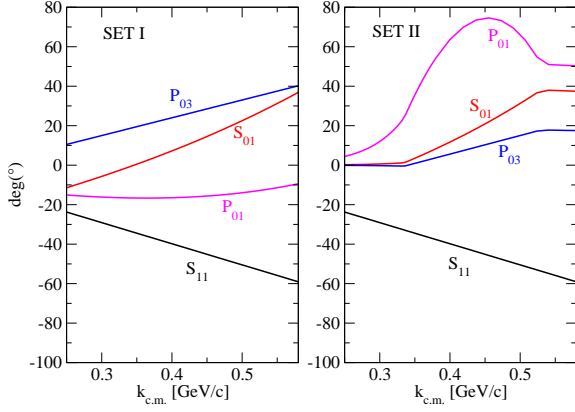


Fig. 5 Phase shifts from the set I (left) and set II (right) vs. kaon c.m. momentum k .

baryon, and our fits from the set II are quite similar to those of Ref. [13].

Figure 5 depicts the phase shift from the set I fitted to Damerell's data, and from the set II fitted to Giacomelli's data, respectively. Based on the S_{11} amplitude in common, the difference is clear between the two sets for the isoscalar amplitudes S_{01} , P_{01} and P_{03} .

In Fig. 6 total cross sections are reproduced for $K^+n \rightarrow K^0p$ and $K^+n \rightarrow K^+n$ reactions by using the set I in the upper panel and by the set II in the lower panel, respectively. The solid and dotted curves represent the success and failure of a given set of parameters for both reaction. The set I agrees with the total cross section for the $K^+n \rightarrow K^0p$ reaction, whereas the set II is consistent with the $K^+n \rightarrow K^+n$ reaction. However, the failure of the set I for the channel $K^+n \rightarrow K^+n$ stands out, as shown by the result of the fit convex down which is reverse to the convex up data. The overestimate for the peak of the $K^+n \rightarrow K^0p$ reaction at $P_{\text{Lab}} \approx 800$ MeV/c implies the disagreement of the set II with experiment either. Thus, the two sets of parameters lead to the result contradictory to each other.

Summarizing what has been obtained from the set I and set II, the total cross sections for $K^+n \rightarrow K^0p$ and $K^+n \rightarrow K^+n$ exhibit a contradiction between the two sets of parameters, which are worse than the case of differential cross sections. In order to find which one is appropriate for both reactions, the polarization observable of K^+N scattering is summoned for this purpose.

For the meson-baryon scattering it is given by [21]

$$P = \frac{2\text{Im}(fg^*)}{|f|^2 + |g|^2}, \quad (20)$$

where f and g are the spin non-flip and spin flip amplitudes, respectively. Polarizations for the reactions $K^+n \rightarrow K^0p$ and $K^+n \rightarrow K^+n$ are presented in Fig. 7 where the solid curve results from the set I, and the dashed one from the set II, respectively. It is interesting

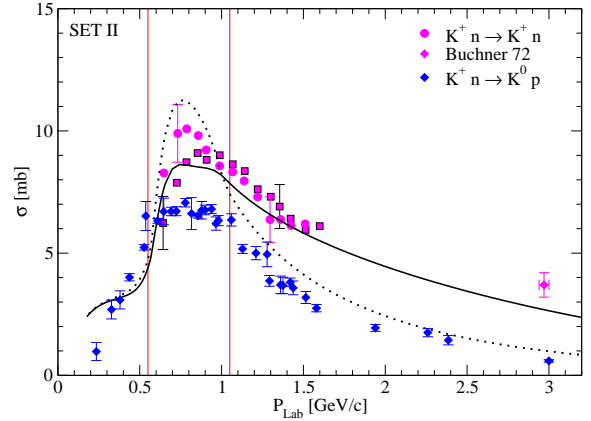
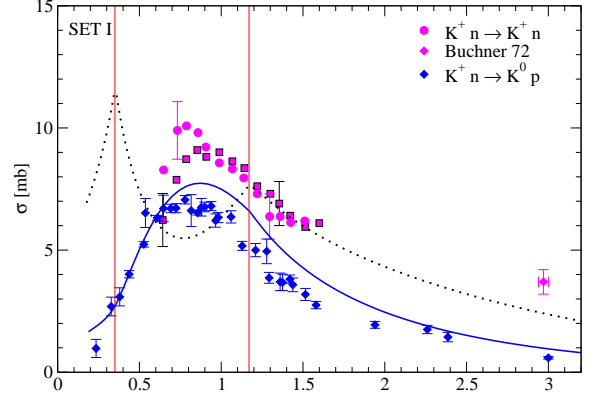


Fig. 6 Total cross sections for the $K^+n \rightarrow K^0p$ and $K^+n \rightarrow K^+n$ reactions from the set I (upper panel) and from the set II (lower panel). The solid (dotted) curve represents the success (failure) of the parameter set given in each panel. Two vertical lines show divisions of the momentum range in our fits discussed in the text. Data are collected from Ref. [16].

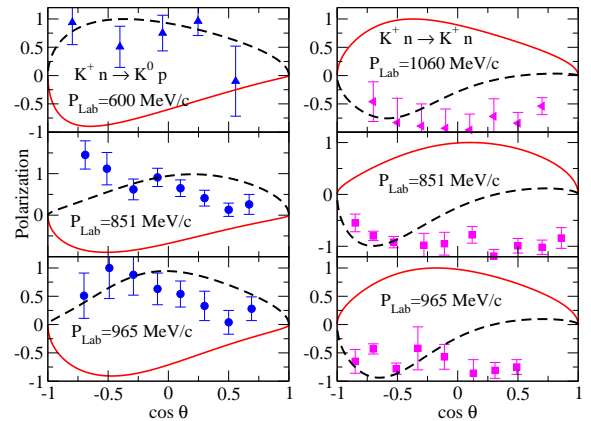


Fig. 7 Polarizations for $K^+n \rightarrow K^0p$ and $K^+n \rightarrow K^+n$ reactions. Solid curves are from the set I, and dashed one from the set II, respectively. Data are taken from Refs. [22, 23, 24, 25].

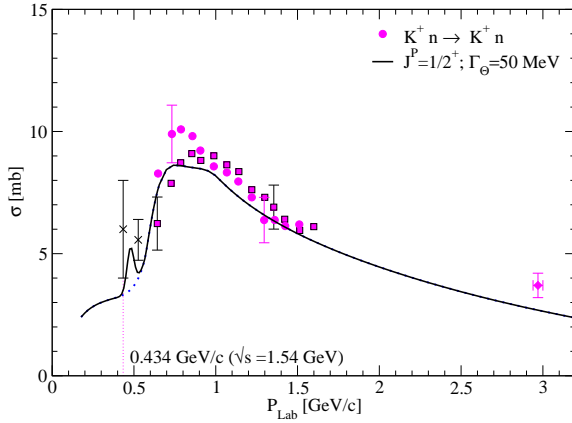


Fig. 8 Total cross section for elastic $K^+n \rightarrow K^+n$ reaction. The solid curve results from the set II and the two points $\sigma = 6 \pm 2$ and 5.6 ± 0.8 [mb] at $P_{\text{Lab}} = 434$ and 526 MeV/c denoted by the vertical bars are obtained by integrating differential cross section data of Ref. [15]. The $\Theta^+(1540)$ peak is shown with parameters as discussed in the text. Data are taken from Ref. [16].

to note that polarizations of $K^+n \rightarrow K^0p$ are positive, whereas they are negative in the case of $K^+n \rightarrow K^+n$. These tendencies continue up to $P_{\text{Lab}} \approx 1500$ MeV/c [22, 23, 24, 25]. Given the sign convention for the polarization in Eq. (20), it is clear that the polarization from the set II is in fair agreement with data. The parameters for the set I lead to the results definitely opposite to the polarization data measured in experiments. The sign of polarization is of significance, because any conclusion obtained could be reversed, if the sign is reversed. We confirm the consistency of the polarization presented in Fig. 7 with those experiments quoted above. Hence, the polarization observable provides a criterion for validating the parameters between the two sets.

4 Discussion

Typically, a resonance would appear in the form of a Bright-Wigner peak in the total cross section at the expected energy. Therefore, the total cross section is easy to check up any profile for the resonance peak. In Fig. 8 total cross section for elastic K^+n scattering is reproduced by using the set II. In addition to empirical data, we introduce the total cross section evaluated at $P_{\text{Lab}} = 434$ MeV/c with the large error bar. It indicates the range of total cross section $4 \leq \sigma \leq 8$ [mb], which is possible from the differential cross section data in Fig. 3. With the maximum value obtained by integrating over the range $-0.85 \leq \cos\theta \leq 0.85$, the minimum is from the integration only in the range $-0.25 \leq \cos\theta \leq 0.65$ where the experimental data exist. For further reference, a second value $4.73 \leq \sigma \leq 6.4$

[mb] at 526 MeV/c is included in the similar fashion. Together with the differential cross sections at $P_{\text{Lab}} = 434$ MeV/c from the set II in Fig. 3, therefore, the result in the total cross section, i.e., $\sigma = 6 \pm 2$ [mb] there, strongly suggests the existence of a resonance around $\sqrt{s} = 1.54$ GeV.

For illustration purpose we finally show the resonance peak at $P_{\text{Lab}} \approx 480$ MeV/c which comes from the Breit-Wigner fit of Ref. [26] with $J^P = 1/2^+$, $M_\Theta = 1555$ MeV, $\Gamma_\Theta = 50$ MeV, $I_R = \sqrt{1/2}$, $X_R = 0.25$ and the damping parameter $d = 1.5$ chosen. A more detailed analysis of the resonance fit with these parameters could help identifying the $\Theta^+(1540)$ baryon further, and should be pursued in future theory and experiments.

Acknowledgments

This work was supported by the National Research Foundation of Korea Grant No. NRF-2017R1A2B4010117.

References

1. R. Aaij *et al.*, arXiv:2006.16957v2.
2. T. Nakano *et al.*, Phys. Rev. Lett. **91**, 012002 (2003).
3. M. J. Amarian *et al.*, Phys. Rev. C **85**, 035209 (2012).
4. D. Diakonov, V. Petrov, and M. Polyakov, Z. Phys. A **359**, 305 (1997).
5. M. Praszalowicz, in: M. Jeżabek, M. Praszalowicz (Eds.), Workshop on Skyrmions and Anomalies, World Scientific, Singapore, 1987, p. 112.
6. R. L. Jaffe, Eur. Phys. J. C **35**, 221 (2004).
7. H. Walliser and H. Weigel, Eur. Phys. J. A **26**, 361 (2006).
8. Takayasu Sekihara, Hyun-Chul Kim and Atsushi Hosaka, Prog. Theor. Exp. Phys., 063D03, 361 (2020).
9. R. A. Arndt, I. I. Strakovsky and R. L. Workman, Nucl. Phys. A **754**, 261c (2005).
10. Ya. I. Azimov, R. A. Arndt, I. I. Strakovsky, R. L. Workman, and K. Goeke, Eur. Phys. J. A **26**, 79 (2005).
11. J. S. Hyslop, R. A. Arndt, L. D. Roper, and R. L. Workman, Phys. Rev. D **46**, 961 (1992).
12. B.-G. Yu and K.-J. Kong, Phys. Rev. C **100**, 065206 (2019).
13. A. Sibirtsev, J. Haidenbauer, S. Krewald, and Ulf-G. Meißner, J. Phys. G: Nucl. Part. Phys. **32**, R395 (2006).
14. K. Aoki and D. Jido, Prog. Theor. Exp. Phys. **2017**, 103D01 (2017).
15. C. J. S. Damerell *et al.*, Nucl. Phys. B **94**, 374 (1975).
16. G. Giacomelli *et al.*, Nucl. Phys. B **56**, 346 (1973).
17. K. Hashimoto, Phys. Rev. C **29**, 1377 (1984).
18. S. Goldhaber, W. Chinowsky, G. Goldhaber, W. Lee, T. O'Halloran, T. F. Stubbs, G. M. Pjerrou, D. H. Stork, and H. K. Ticho, Phys. Rev. Lett. **9**, 135 (1962).
19. W. Cameron *et al.*, Nucl. Phys. B **78**, 93 (1974).
20. C. J. Adams *et al.*, Nucl. Phys. B **66**, 36 (1973).
21. G. Giacomelli *et al.*, Nucl. Phys. B **71**, 138 (1974).
22. A. K. Ray *et al.*, Phys. Rev. **183**, 1183 (1969).
23. K. Nakajima *et al.*, Phys. Lett. B **112**, 75 (1982).
24. A. W. Robertson *et al.*, Phys. Lett. B **91**, 465 (1980).
25. S. J. Watts *et al.*, Phys. Lett. B **95**, 323 (1980).
26. K.-J. Kong and B.-G. Yu, Phys. Rev. C **98**, 045207 (2018).